CONF-9009381--1

DE91 012228

AN ASSESSMENT OF THE LIFETIME OF FARADAY SHIELD ELEMENTS*

J. B. O. Caughman, II, and D. N. Ruzic
University of Illinois, Urbana, Illinois 61801
D. J. Hoffman, R. A. Langley, M. B. Lewis, and P. M. Ryan
Oak Ridge National Laboratory, Oak Ridge, Tennessee 37831-8071

ABSTRACT

The interaction of plasma with rf fields from an ion cyclotron range of frequencies (ICRF) antenna has been studied to estimate the amount of Faraday shield erosion expected in normal ICRF heating (ICRH) operation. Plasma parameters and ion energies have been measured in the near field of an antenna and used in a model to estimate the erosion rate of the Faraday shield surface. Experiments were conducted on the RF Test Facility (RFTF), a magnetic mirror device at Oak Ridge National Laboratory (ORNL), using a single-strap resonant loop antenna with a two-tier Faraday shield. The outer tier, facing the plasma, was layered with graphite tiles. The antenna was operated at currents and voltages (~500 A, ~20 kV at 25 kW) within 50% of those expected in tokamaks. The time-varying floating potential was measured with a capacitively coupled probe, and the time-averaged floating potential, electron temperature, and electron density were measured with a Langmuir probe. Both probes were scanned in front of the antenna. Ion energies were measured with a gridded energy analyser located below the antenna, and samples of silicon were placed on the Faraday shield surface to estimate the incident ion energy. The capacitive probe measurements show that the rf floating potential follows the magnetic field pattern of the antenna, indicating that the electromagnetic fields are responsible for the potential formation. Electron temperatures increase with rf power and can reach values $\geq$60 eV for an rf power of ~25 kW. Incident ion energies $\geq$300 eV have been measured for the same power level. Plasma parameters and ion energies have been correlated with the antenna current and used in a computational model of the plasma sheath to predict the amount of erosion expected from the Faraday shield elements exposed to plasma. Predictions of light ion sputtering of candidate Faraday shield materials are presented.

INTRODUCTION

Experiments on several confinement devices have shown an increase in the impurity concentration in the plasma during ICRH [1-7]. Specifically, the Faraday shield of the antenna has been identified as a local impurity source [8,9]. The increase in the impurity release from the antenna will decrease its lifetime because of the erosion of its plasma facing components. Therefore, the processes taking place at the antenna that cause the increase in the impurity generation must be identified. One area that needs to be addressed in understanding the impurity generation is the role of the plasma sheath that forms on the material boundaries in contact with the plasma. Ions are accelerated through the sheath and hit the antenna, causing material erosion. The magnitude and form of the plasma potential in front of the antenna must be known to determine the effect of this potential on the energy of the ions hitting the shield. The effect of the electron temperature and the rf fields on the potential formation in front of the antenna must be determined.

Plasma parameters and ion energies have been measured near an ICRF antenna Faraday shield in an experiment conducted on the RFTF at ORNL [10]. The antenna used was a single-strap resonant loop antenna with a grounded two-tier Faraday shield, shown in Fig. 1. The antenna was operated at 42 MHz, and the

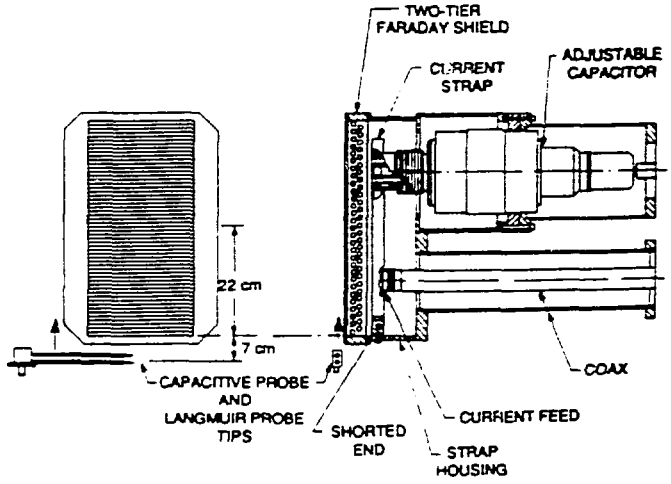

Fig. 1. Front and sectional views of the resonant loop antenna, showing the position of the probes relative to the Faraday shield.

Research supported by the Magnetic Fusion Energy Technology Fellowship program, administered by Oak Ridge Associated Universities for the U.S. Department of Energy, and the Office of Fusion Energy, U.S. Department of Energy, under contract DE-AC05-84OR21400 and subcontract 19X-SB359V with Martin Marietta Energy Systems, Inc.

rf power was varied up to 60 kW. The RFTF plasma was initiated and sustained by electron cyclotron heating (ECH) using a 10.6-GHz klystron with an output power of ~17 kW. Typically, the plasma discharge was pulsed for 200 ms, and the antenna was pulsed for 150 ms during the plasma pulse. Hydrogen was used as the operating gas for most of the experiments at pressures ranging from 1×10^{-4} to 4×10^{-4} Torr. The electron temperature at the antenna was 5–10 eV, and the electron density was $\sim 5 \times 10^{10}$ cm^{-3}. The magnetic field at the antenna was ~2 kG and in a direction parallel to the Faraday shield elements.

EXPERIMENT

The time-varying floating potential was measured with a capacitively coupled probe that was scanned in front of the antenna, parallel to the current strap, from 7 cm below the shorted end of the current strap to 22 cm above the shorted end. The probe was calibrated at the rf frequency (42 MHz) [11]. A Langmuir probe was scanned in the same area as the capacitive probe to measure the time-averaged floating potential, electron temperature, and electron density. Both probe tips were ~1 cm from the surface of the Faraday shield. The response of the Langmuir probe in the presence of rf fields was considered in the analysis of the probe characteristics. The Langmuir probe was terminated on a small dc and rf load and thus measured the time-averaged current as a function of applied bias voltage. The electron temperature was taken from the lower portion of the I_e vs V curve to avoid problems associated with response of a Langmuir probe to an rf plasma [12]. The electron density was calculated by measuring the probe current well into ion saturation and then corrected with the LaFramboise method [13]. The time-averaged floating potential was taken from the time-averaged current measurement and then corrected for self-bias due to rf effects [14]. The time-averaged plasma potential was estimated from the $\ln(I_e)$ vs V_{bias} curve [15].

A gridded energy analyzer, located ~4 cm below the antenna and facing the plasma, measured the distribution of ion energies incident on a grounded surface. Since the magnetic field was parallel to the surface and to the biasing grids of the analyzer, the analyzer was thin ($\leq$1 mm thick) so that the ion energies perpendicular to the magnetic field could be measured. The outside of the analyzer and its entrance grid were grounded, so that the energy of the ions accelerated through the sheath that formed on a grounded surface was measured.

Samples of silicon were placed on and near the antenna to estimate the energy of the ions accelerated through the plasma sheaths that formed on surfaces. Some samples were placed in the same location as the energy analyzer, and some were placed on the Faraday shield surface at a location ~16 cm from the shorted end of the antenna. Some of the samples were exposed only to ECH plasmas; some were exposed to ECH plasmas with rf power radiating from the antenna. The samples were exposed to a near-saturation fluence ($\sim 5 \times 10^{17}$ D/cm^{-3}) from a deuterium plasma. The incident fluence was estimated by measuring the current to the samples. The amount of deuterium retained in the samples after exposure to saturation levels of a deuterium ion fluence is related to the energy of the incident ions [16] and was determined by using D(^{3}He,p)^{4}He nuclear reaction analysis.

RESULTS

The capacitive probe results indicate that the floating potential near the antenna oscillates at the rf frequency and can reach values of up to 300 V p-p for an antenna current of ~400 A. The rf floating potential, normalized by the antenna current, is shown in Fig. 2 for gas pressures of (1–3) $\times 10^{-4}$ Torr and for rf powers ranging from 12 to 55 kW. The potentials are all measured ~1 cm in front of the Faraday shield and are referenced from the shorted end of the antenna. Since the rf field strength is proportional to the antenna current, the potentials were normalized by the antenna current to look for any dependence on the rf field strength. The waveform of the potential was sinusoidal for all cases. For each data set at the same pressure, the data show the trend of being fairly level in the middle of the current strap and decreasing slightly towards the ends of the strap. These potentials follow the magnetic field

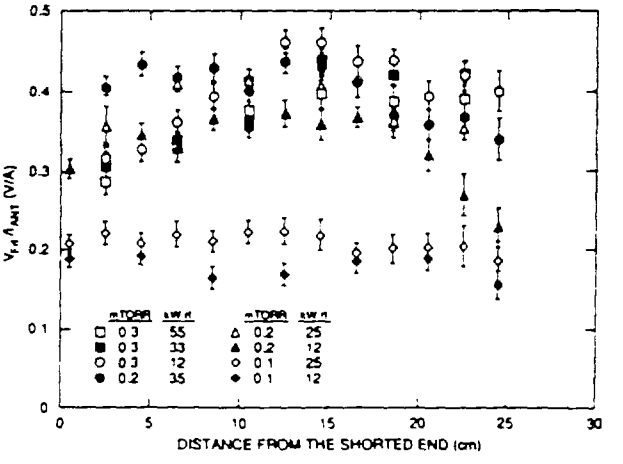

Fig. 2. The rf component of the floating potential normalized by the antenna current.

pattern of the antenna instead of the voltage distribution on the current strap, indicating that the potential formation was due to the electromagnetic fields and not the electrostatic fields.

The difference between the normalized potentials for the 1×10^{-4} Torr experiment and the $(2\text{–}3) \times 10^{-4}$ Torr experiments may be due to the capacitance of the rf sheath at the probe tip. The sheath capacitance acts as a series capacitor between the probe tip and the plasma and decreases the coupled signal to the probe tip. The sheath capacitance will increase as the electron density increases because the sheath thickness is thinner, and the coupled voltage to the probe tip will increase. The plasma densities were lower for the lower gas pressures, typically $(1\text{–}3) \times 10^{10}$ cm^{-3} for the 1×10^{-4} Torr experiment, and increased to $(8\text{–}16) \times 10^{10}$ cm^{-3} for the 4×10^{-4} Torr experiment.

The electron temperature and the time-averaged plasma potential in front of the antenna are shown in Fig. 3 for a gas fill pressure of 2×10^{-4} Torr. Also shown are data from below the antenna, close to the energy analyzer. The electron temperature and the plasma potential clearly increase with rf power and antenna current. Electron temperatures for an ECH plasma without rf power from the antenna were 5–10 eV (curve 1) and increased to 54–60 eV for an ECH plasma with an applied rf power of ~26 kW and an antenna current of ~390 A; the average plasma potential for an ECH plasma without rf power from the antenna was 7–12 V (curve 1) and increased to 180–230 V for these rf conditions. Both the electron temperature and the average plasma potential were fairly constant in front of the antenna, indicating an electromagnetic field dependence.

There was no clear dependence of the electron temperature or the plasma potential on the local electron density. Without rf power from the antenna, the plasma densities were $(3\text{–}5) \times 10^{10}$ cm^{-3} in front of the antenna and about 7×10^{10} cm^{-3} below it. The electron density in front of the antenna decreased ~50% at lower rf power and 25–50% at higher rf power. The density below the antenna decreased ~25% for the lower rf power case and increased ~50% with higher rf power. Even though the density increased, the electron temperature and the average plasma potential followed a scaling similar to that of the parameters in front of the antenna. Experiments at 4×10^{-4} Torr showed that the temperature and potential scaled with the antenna current in the same way, even though the density in front of the antenna increased 100 to 150% for an rf power of ~11.2 kW.

Energies for ions hitting a grounded surface also increased with rf power and antenna current. The perpendicular ion energy distribution measured with the

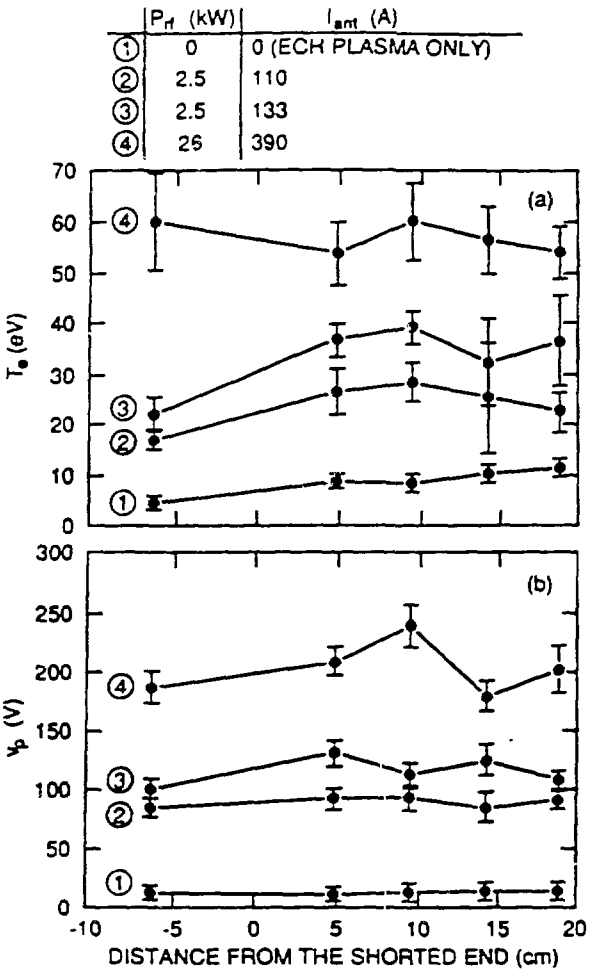

Fig. 3. (a) Electron temperature and (b) average plasma potential in front of the antenna for a gas pressure of 2×10^{-4} Torr.

energy analyzer is shown in Fig. 4 for the three sets of plasma and antenna conditions. The fine structure of the distributions is not meaningful because of the uncertainty involved in the measurement. The distributions were normalized so that the integral over the energy was one. The ion energy distributions were generally peaked near the time-averaged plasma potential for all the experiments. Energy distributions were peaked at 5–10 eV for the experiments without rf and increased with rf power. Ions with energies above 300 eV were measured for experiments with an rf power of ~20 kW and an antenna current of ~400 A. The distributions were clearly shifted to higher energies with the higher rf power and antenna current. The magnitude of the energy shift follows roughly the same scaling as the electron temperature increase, indicating that the electrons

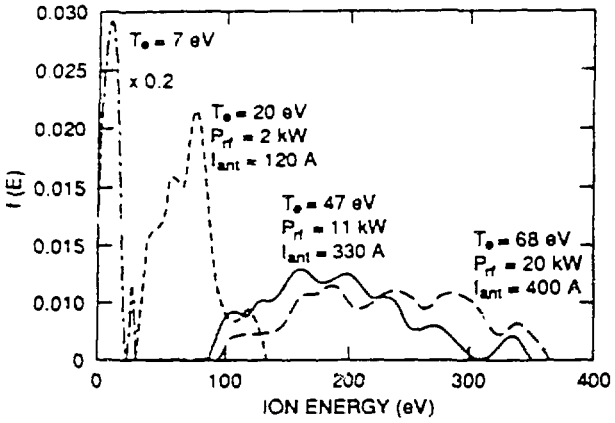

Fig. 4. Measured perpendicular ion energy distributions for a gas pressure of 2×10^{-4} Torr.

caused an increase in the sheath potential, thereby increasing the energy of the ions that hit the surface.

The surface probe results for the experiments are shown in Fig. 5. Some of the samples were negatively biased and exposed to deuterium plasmas without rf power from the antenna. The negative bias allowed the ions to have an equivalent energy of the plasma potential (~20 V) plus the magnitude of the applied bias voltage. The amounts of deuterium trapped in the biased samples for various incident fluences are shown as the solid points in the figure. The amount of trapped deuterium was within the range of previous experimental results for monoenergetic deuterium incident on silicon [16], shown as dotted lines in the figure.

The samples exposed to a plasma with rf power from the antenna had more trapped deuterium than the sample with the −250-V bias, indicating an increase in the

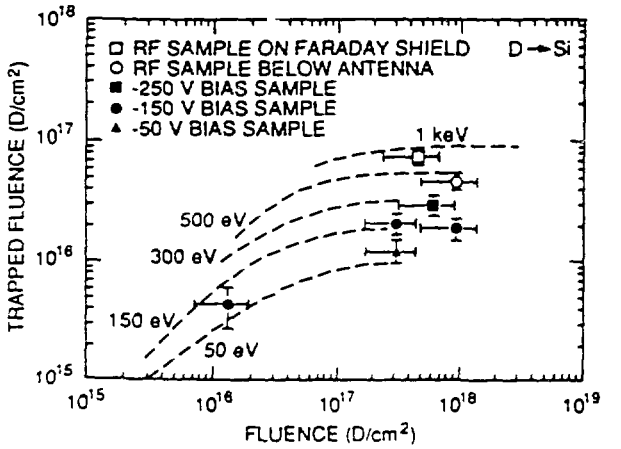

Fig. 5. Nuclear reaction analysis data for the experiment. Also shown are the monoenergetic results (dotted lines [16]).

ion energy hitting the surface. One sample (grounded) was at the same location as the biased samples (~4 cm below the antenna), and the other sample was in the middle of the Faraday shield of the antenna, ~16 cm from the shorted end of the current strap. The rf power was ~22 kW, and the antenna current was ~269 A. Although the amounts of trapped deuterium in these samples were greater than in the −250-V bias sample (ion energy ~ 270 eV), it does not mean that all the ions had an energy greater than 270 eV. The ion energy distribution will affect how much is retained, as well as the impact angle [17]. Higher energy ions from the distribution can cause the trapped amounts to increase [16]. Since the exact distribution is not known, these results should be interpreted as indicating that, for these experimental conditions, some of the ions hitting the Faraday shield had an energy above 270 eV.

DISCUSSION

The electron temperature, plasma potential, and impacting ion energy in the region in front of the antenna clearly increase with antenna current and near-field strength. The increase in the ion energies measured with the energy analyzer is consistent with an increased sheath potential resulting from an increase in the electron temperature. These large potentials, coupled with the acceleration of the ions through the resulting sheath, will cause an increase in the amount of erosion from the Faraday shield because of the increase in the energy of the ions hitting the shield surface.

A computational model of the sheath has been developed to estimate the energy of the ions incident on the Faraday shield surface [15]. Inputs to the model include measured data, such as the magnitude of the time-varying plasma potential, the time-averaged plasma potential, and the electron temperature. Other inputs are the static magnetic field strength, the electron density, and the ion temperature. As an example of the model, the measured data from the RFTF experiment (Figs. 2–4) were scaled up with antenna current to estimate the conditions that may exist directly in front of an antenna in a large tokamak, such as TFTR or JET. For an antenna current of 800 A, the inputs to the model for the tokamak-like conditions were an average plasma potential of 480 V, a time-varying plasma potential of 130 V, and an electron temperature of 110 eV. The electron density was assumed to be 1×10^{13} cm^{-3}, the magnetic field was 3.6 T, the ion temperature was 37 eV, the rf frequency was 47 MHz, and the plasma was assumed to be deuterium. The results of the model for these conditions are shown in Fig. 6. The fine structure is due to numerical uncertainties in the calculation. The peak in the ion energy distribution occurs near the peak in the plasma potential. This

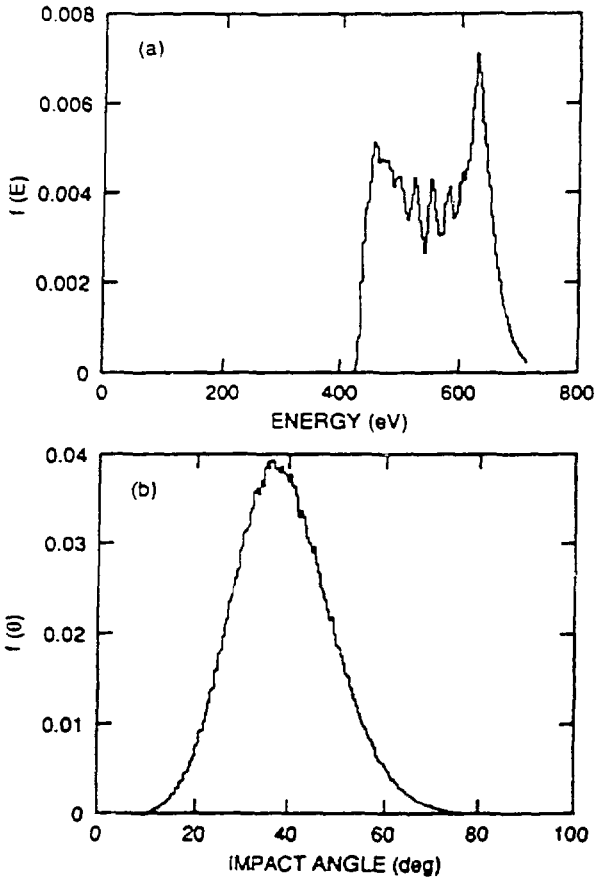

Fig. 6. Calculated (a) ion energy distribution and (b) ion angular distribution at the surface for tokamak-like conditions. Input parameters for the calculation were a dc plasma potential of 480 V, an rf potential of 130 V, $n_e = 1.0 \times 10^{12}$ cm^{-3}, $T_e = 110$ eV, $T_i = 37$ eV, an rf frequency of 47 MHz, and a magnetic field strength of 3.6 T.

population of higher energy ions will increase the effective sputtering yield of the ions incident on the Faraday shield surface. The sputtering yield is also affected by the ion impact angle. The model results show that the average angle at which the ions will hit the shield is 39°.

The decrease in the lifetime of the Faraday shield due to physical sputtering can be calculated from the results of the computational model for light ion sputtering of various Faraday shield materials. The calculated ion energy distribution at the Faraday shield surface for the tokamak-like conditions described above was used in an analytical expression for calculating the sputtering yield for deuterium sputtering of beryllium, copper, nickel, titanium carbide, and graphite [18]. This analytical expression is typically accurate to within a factor of two. The angular dependence on the sputtering yield was approximated as having a $1/\cos(\theta)$ distribution for ion energies greater than 200 eV. The results of this calculation are shown in Table I. For comparison, the ion energy distribution at the surface without rf effects was approximated as being a half-Maxwellian ($T_i = T_e$) shifted by the sheath potential ($\sim 3T_e$). No angular dependence was assumed. Results from the analytical sputtering formula for this distribution for electron temperatures of 20 eV and 10 eV are also shown in Table I. The sputtering yields for the rf conditions (Fig. 6) are higher than those for the non-rf conditions. Compared to the 20-eV electron temperature calculation, the yield increases ranged from a factor of 1.7 for deuterium sputtering of beryllium up to a factor of 8.5 for deuterium sputtering of TiC.

The erosion rate of the Faraday shield has been calculated from the sputtering yields shown in Table I. The erosion rate is given by the product of the incident ion flux, the sputtering yield, and the number density of the Faraday shield material. The number density was calculated as the mass density multiplied by 6.023×10^{23} and divided by the atomic/molecular mass [19]. The erosion rates are also shown in Table I. These results were calculated for an incident flux of 1×10^{17} ions/cm^2·s. The erosion rates are about the same for the deuterium sputtering of beryllium, titanium carbide, and graphite; they are higher for copper and nickel. At this incident flux, the plasma-facing antenna components in a tokamak run for 30-s pulses would erode ~1 mm after ~108,000 pulses (for beryllium). This calculation does not include the effects of self-sputtering. Sputtering yields for the rf conditions would increase by more than an order of magnitude for self-sputtering, also increasing the erosion rate.

CONCLUSIONS

Experiments have shown that large plasma potentials exist in front of an ICRF antenna. Electron temperatures, plasma potentials, and ion energies clearly increase with antenna current and generally follow the near-field magnetic field pattern of the antenna, indicating that the increases in potential and temperature are due to the electromagnetic field and not the electrostatic field. The time-averaged plasma potential follows the same scaling as the electron temperature, indicating that the increase in sheath potential is due to an increase in the electron temperature. This increased sheath potential causes an increase in the energy of the ions hitting the plasma-facing components of the antenna. Calculations of the distribution of ion energies at a grounded surface show that the ions will hit the surface with a spread in energies that is peaked near the maximum plasma potential for tokamak-like conditions. Sputtering yields and erosion rates will increase

Table I. Calculated sputtering yields and erosion rates for deuterium sputtering of Faraday shield materials

	Material				
	Be	Cu	Ni	TiC	Graphite
Sputtering yield (atoms/ion)					
Conditions of Fig. 6	3.82×10^{-2}	1.06×10^{-1}	5.63×10^{-2}	1.91×10^{-2}	4.81×10^{-2}
No rf, $T_e = 20$ eV	2.27×10^{-2}	7.94×10^{-3}	8.66×10^{-3}	2.25×10^{-3}	1.54×10^{-2}
No rf, $T_e = 10$ eV	6.21×10^{-3}	3.99×10^{-4}	6.66×10^{-4}	2.05×10^{-4}	2.59×10^{-3}
Erosion rate[a] (cm/s)					
Conditions of Fig. 6	3.08×10^{-8}	1.25×10^{-7}	6.17×10^{-8}	3.85×10^{-8}	5.33×10^{-8}
No rf, $T_e = 20$ eV	1.83×10^{-8}	9.35×10^{-9}	7.29×10^{-9}	4.53×10^{-9}	1.71×10^{-8}
No rf, $T_e = 10$ eV	5.01×10^{-9}	4.02×10^{-10}	7.26×10^{-10}	1.71×10^{-8}	2.87×10^{-9}

[a]For a flux of 10^{17} D^+/cm^2.

for these conditions, limiting the lifetime of the plasma-facing components of the antenna.

REFERENCES

[1] K. H. Behringer et al., in *Proc. 13th European Conf. Controlled Fusion and Plasma Heating*, Schliersee, 1986, p. 176.

[2] J. Tachon, in *Physics of Plasma-Wall Interactions in Controlled Fusion*, eds. D. E. Post and R. Behrisch. New York: Plenum, 1986, p. 1005.

[3] G. Janeschitz et al., in *Proc. 13th European Conf. Controlled Fusion and Plasma Heating*, Schliersee, 1986, p. 407.

[4] B. Schweer et al., ibid., p. 399.

[5] A. deChambrier et al., J. Nucl. Mater., vols. 128 & 129, p. 310, 1984.

[6] H. Ogawa et al., J. Nucl. Mater., vols. 128 & 129, p. 298, 1984.

[7] H. L. Manning et al., Nucl. Fusion, vol. 26, p. 1665, 1986.

[8] M. Bureš et al., Plasma Phys. Controlled Fusion, vol. 30, p. 149, 1988.

[9] J.-M. Noterdaeme et al., in *Proc. 14th European Conf. Controlled Fusion and Plasma Heating*, Madrid, 1987, p. 678.

[10] W. L. Gardner et al., Bull. Am. Phys. Soc., vol. 30, p. 1590, 1985.

[11] J. B. O. Caughman, II, D. N. Rusic, and D. J. Hoffman, J. Vac. Sci. Technol. A, vol. 7, p. 1092, 1989.

[12] N. Hershkowitz, M. H. Cho, C. H. Nam, and T. Intrator, Plasma Chem. Plasma Process., vol. 8, p. 35, 1988.

[13] P. M. Chung, L. Talbot, and K. J. Touryan, *Electric Probes in Stationary and Flowing Plasmas: Theory and Application*. New York: Springer-Verlag, 1975.

[14] A. Boschi and F. Magistrelli, Nuovo Cimento, vol. 29, p. 487, 1963.

[15] J. B. O. Caughman, II, Ph.D. thesis, University of Illinois at Urbana-Champaign, October 1989.

[16] G. Staudenmaier et al., J. Nucl. Mater., vol. 84, p. 149, 1979.

[17] S. A. Cohen and G. M. McCracken, J. Nucl. Mater., vol. 84, p. 157, 1979.

[18] J. Bohdansky, p. 61 in *Data Compendium for Plasma-Surface Interactions*, Nucl. Fusion, Special Issue, 1984.

[19] *CRC Handbook of Chemistry and Physics*, 59th ed. West Palm Beach: CRC Press, 1978.